J. Phys. B: At. Mol. Opt. Phys. **29** (1996) 1723–1736. Printed in the UK

A classical analysis of proton collisions with ground-state and excited, aligned sodium targets

C J Lundy and R E Olson

Physics Department, University of Missouri-Rolla, Rolla, MO 65401, USA

Received 27 November 1995, in final form 1 January 1996

Abstract. The dependence of electron capture and ionization processes on the pre-collision electronic distribution is examined for the systems $H^+ + Na(3s, 3p\Sigma, 3p\Pi)$ primarily in the energy range 1–15 keV. Populations of the capture and ionization channels as well as the coherence of the post-collision electronic distribution of the capture product are formulated using the classical trajectory Monte Carlo (CTMC) method. Total capture and ionization cross sections arising from initially aligned Na(3p) targets exhibit transient behaviour near the velocity-matching energy of 5.7 keV. This observation is described in terms of anisotropy parameters; anisotropy effects are also analysed for the capture states $n = 2$, 3 and 4. In addition to the population manifold, we present theoretical calculations of the alignment parameter A_{20} and the z-component of the dipole moment $\langle \boldsymbol{D}_z \rangle$, in order to relate the alignment of the post-collision charge cloud to that of the initial Na(3s, 3pΣ, 3pΠ) target states. The z-component of the cross product of the angular momentum and the Runge–Lenz vector $\langle (\boldsymbol{L} \times \boldsymbol{A})_z \rangle$ is used to describe the orientation of the post-collision product generated from the aligned Na(3pΣ, 3pΠ) pre-collision reactants.

1. Introduction

In a collision event, the electronic charge distribution carries information concerning the dynamics of the interaction. The description of the charge cloud is classified in terms of *alignment* which characterizes the spatial distribution and also *orientation* or rotation of the charge cloud. In terms of the magnetic-substate populations, an alignment represents a symmetric distribution about $m_\ell = 0$ while an asymmetric distribution about $m_L = 0$ indicates an orientation. In order to examine the progression of the charge cloud during a collision event, knowledge of its initial state is fundamental. Experimentally, this is accomplished via optical pumping with linearly polarized light to prepare excited atoms with alignment of the magnetic substates and with circularly polarized light to define an orientation. Sodium is a favourite prototype for experimental measurements since it can easily be pumped into the Na(3p) state using a dye-laser tuned to the Na D-line (wavelength of 589 nm) (Fischer and Hertel 1982, Hertel and Stoll 1978). It is also a favourite for theoretical studies since sodium essentially behaves like a one-electron atom. These observations and calculations can thus yield an insight into the behaviour of the collision mechanisms when the electronic cloud is parallel ($3p\Sigma$) to the projectile velocity vector or perpendicular ($3p\Pi$) to it. To this end, we simulate $H^+ + Na(3s, 3p\Sigma, 3p\Pi)$ collisions using the classical trajectory Monte Carlo (CTMC) method which retains the coordinate and momentum vectors of the electron throughout the collision event. Hence, this method inherently provides information regarding the shape and rotation of the statistically generated charge cloud during the course of the collision process.

0953-4075/96/091723+14$19.50

Considerable cross sectional data exist for proton collisions with ground-state sodium atoms (Aumayr *et al* 1987 and references therein). Recently, Roller-Lutz *et al* (1993) have measured the polarization and orientation characteristics differential in scattering angle for the H(2p) product. With a spherically symmetric Na(3s) initial charge distribution, they observed a definite preference for an alignment in the direction of the impact velocity vector for the final charge distribution at small scattering angles, less than 0.1°. In addition, they reported a decrease in the magnitude of the angular momentum perpendicular to the scattering plane in this angular regime where approximately 80% of the (2p) capture population occurs.

For $H^+ + Na(3p\Sigma, 3p\Pi)$ collisions, Dowek *et al* (1990) have performed measurements displaying the relative populations of state-selective electron capture from the initially-aligned sodium targets at low energies. They observed a 3:2 ratio favouring capture to $H(n = 2)$ from $Na(3p\Sigma)$ versus $Na(3p\Pi)$ for energies at and below 2 keV; however, the relative populations for capture to higher excited states showed a strong energy dependence with dominating cross sections arising from $Na(3p\Pi)$ above 1 keV. Results of Müller *et al* (1995) for cross section ratios arising from total capture indicated similar energy behaviour with a cross-over occurring at the energy at which the projectile velocity equals that of the orbiting target electron, i.e. the velocity-matching energy. At 1 keV, cross sections (Richter *et al* 1993) for capture to $H(n = 2)$ from $Na(3p\Sigma)$ and $Na(3p\Pi)$ and anisotropy or relative cross section measurements (Wang *et al* 1994) differential in scattering angle have further shown a preference for capture from $Na(3p\Sigma)$ at small angles.

The goal of this study is to present a theoretical framework which extends beyond the impact energy of 2 keV at which most experimental results for the proton–sodium system reside. The cross-sectional data is benchmarked with available experimental measurements, and coherence parameters are calculated which identify the nature of the electronic spatial distribution before and after the collision. Several modes of parametrization for alignment studies exist (Andersen *et al* 1988, Andersen and Hertel 1986, Hippler 1993). We have chosen to describe the shape of the charge distribution in terms of the electric dipole moment and the alignment parameter A_{20}. The frame of reference used in this study is the standard collision frame with the collision velocity and the impact-parameter vectors defining the z-axis and x-axis, respectively. x- and z-components of the dipole moment fix the tilt and eccentricity of the electronic orbit in the xz-scattering plane. In particular, a positive z-component of the dipole moment $\langle \boldsymbol{D}_z \rangle$ indicates a charge cloud lagging behind the projectile while an electron cloud preceding the projectile will yield a negative $\langle \boldsymbol{D}_z \rangle$. When the impact parameters are confined to the positive x-axis, $\langle \boldsymbol{D}_x \rangle$ will generally be non-zero. The alignment parameter A_{20} reflects the alignment of the electronic distribution with respect to the directions parallel and perpendicular to the incident velocity vector; that is, it yields the relative populations of the magnetic substates for 2p production (Hippler *et al* 1986)

$$A_{20} = \frac{\sigma_1 - \sigma_0}{\sigma_{2p}} \tag{1}$$

where σ_0 represents the $m_\ell = 0$ population, σ_1 is the average of the $m_\ell = 1$ and $m_\ell = -1$ populations, and σ_{2p} corresponds to the (2p) cross section. The linear polarization P is related to A_{20} (Hippler *et al* 1986),

$$P = \frac{3A_{20}}{A_{20} - 6}\,. \tag{2}$$

Although both A_{20} and $\langle \boldsymbol{D}_z \rangle$ characterize the concept of alignment, they are complementary rather than repetitive in this description. For parametrization of the orientation, $\langle (\boldsymbol{L} \times \boldsymbol{A})_z \rangle$

points in the direction of the orbital velocity at the perihelion.

By nature of the CTMC method, all reaction channels are represented which not only permits treatment of the capture process for impact energies above 2 keV but also allows investigation of initial alignment of the charge distribution on the ionization channel. We compare our CTMC results for $H^+ + Na(3s)$ with the quantum mechanical calculations of Jain and Winter (1995) and present ionization cross sections generated from proton interaction with $Na(3p\Sigma)$ and $Na(3p\Pi)$ to encourage further experimental study.

2. Theoretical method

The CTMC method is based on iteratively solving Hamilton's equations of motion in which we use an analytic Hartree–Fock potential (Garvey *et al* 1975) to account for screening of sodium's non-valence electrons. The CTMC method is well represented in the literature (refer to Olson and Salop 1977 for a detailed description). Moreover, it has been successfully applied to the prediction of cross sections for capture from aligned sodium targets with multiply charged projectiles (Schlatmann *et al* 1993) and the polarization of product states in $He^{++} + Na(3s)$ collisions (Schippers *et al* 1995). Further, low-energy cross sections for capture from oriented sodium atoms have been calculated by Lewartowski and Courbin (1992), and $\langle \boldsymbol{D}_z \rangle$ and $\langle (\boldsymbol{L} \times \boldsymbol{A})_z \rangle$ results for proton–helium collisions have been given by Lundy *et al* (1994).

In the CTMC theoretical framework, a Na(3p) state is constructed with a binding energy of 0.111 56 (au) and by restricting the angular momentum (L_c) of the electron relative to the Na core (Becker and MacKeller 1984),

$$\ell \leqslant L_c < \ell + 1 \qquad \text{(p-state: } \ell = 1)\,. \tag{3}$$

To obtain a given m_ℓ substate, the electronic orbits are fixed in the xy, xz or yz planes such that the z-component of the angular momentum (L_z) is effectively quantized,

$$\begin{aligned} (xy) &\Rightarrow L_z = \pm 1 \\ (xz) &\Rightarrow L_z = 0 \\ (yz) &\Rightarrow L_z = 0\,. \end{aligned} \tag{4}$$

In the collision frame, the sigma and pi states are formed from the instances where the x, y and z components of angular momentum are set equal to zero,

$$\begin{aligned} \sigma_\Sigma &= (\ell_z = 0) \\ \sigma_\Pi &= \tfrac{1}{2}[(\ell_x = 0) + (\ell_y = 0)]\,. \end{aligned} \tag{5}$$

A sigma cross section then corresponds to a population generated when the component of angular momentum along the direction of the collision velocity vector is zero. Likewise, a pi state is constructed by averaging the two cases where $(\ell_i = 0)$ for projections in the axial directions perpendicular to the ion beam. These cases where the x, y and z components of angular momentum are zero correspond to an average of the two orthogonal planes which share the x-, y- and z-axis, respectively

$$\begin{aligned} (\ell_z = 0) &= \tfrac{1}{2}(\sigma_{xz} + \sigma_{yz}) \\ (\ell_x = 0) &= \tfrac{1}{2}(\sigma_{xz} + \sigma_{xy}) \\ (\ell_y = 0) &= \tfrac{1}{2}(\sigma_{xy} + \sigma_{yz})\,. \end{aligned} \tag{6}$$

In terms of the planar configurations, sigma and pi cross sections are given as

$$\sigma_\Sigma = \tfrac{1}{2}(\sigma_{xz} + \sigma_{yz})$$
$$\sigma_\Pi = \tfrac{1}{2}\sigma_{xy} + \tfrac{1}{4}(\sigma_{xz} + \sigma_{yz})\,. \tag{7}$$

It is also important to note that sigma and pi satisfy the correct degeneracy of the (3p) state and that the spatial dimensions are equivalent:

$$\sigma_{3\mathrm{p}} = \tfrac{1}{3}(2\sigma_\Pi + \sigma_\Sigma) = \tfrac{1}{3}(\sigma_{xy} + \sigma_{xz} + \sigma_{yz})\,. \tag{8}$$

For the initial state Na(3pΠ), the alignment of the product H(2p) will depend on the azimuthal angle of the pre-collision distribution. The magnetic substate populations are calculated for the azimuthal angles $\phi = 0^\circ$, 45° and 90° by setting the appropriate components of the angular momentum equal to zero

$$\Pi(\phi = 0^\circ) = (\ell_x = 0)$$
$$\Pi(\phi = 45^\circ) = \tfrac{1}{2}[(\ell_x = 0) + (\ell_y = 0)] \tag{9}$$
$$\Pi(\phi = 90^\circ) = (\ell_y = 0)$$

and again using (6) to obtain the cross sections in terms of the planar configurations.

In the classical description of the post-collision capture product, $\langle \boldsymbol{D}_z \rangle$ and $\langle \boldsymbol{D}_x \rangle$ are the negated z- and x-coordinates, respectively, of the time-averaged electron position relative to the projectile for an ensemble of trajectories. The $\langle \boldsymbol{D}_z \rangle$ characterization represents a statistical average of the forward–backward asymmetry formed from an ensemble of given capture events; likewise, $\langle \boldsymbol{D}_x \rangle$ describes the up–down asymmetry with respect to an incoming projectile along the positive x-axis. The alignment angle is calculated in terms of these components of the dipole moment—that is, the angle which is formed by the semi-major axis of the characteristic orbit and the z-axis,

$$\gamma = a\tan\frac{\langle \boldsymbol{D}_x \rangle}{\langle \boldsymbol{D}_z \rangle}\,. \tag{10}$$

In order to determine the direction of rotation for the post-collision electronic orbit, the Runge–Lenz vector must first be calculated (Burgdörfer 1983),

$$\boldsymbol{A} = [(\boldsymbol{p} \times \boldsymbol{L}) - Z_\mathrm{p}\mu\boldsymbol{r}/r][-2muE_\mathrm{p}]^{1/2} \tag{11}$$

where p, L and r refer to the linear momentum, angular momentum and radial distance, respectively, of the captured electron with respect to the projectile. Z_p is the charge of the projectile, μ is the reduced mass of the collision product, and E_p is the binding energy of the electron. From this constant of motion $\boldsymbol{A}$ and the angular momentum $\boldsymbol{L}$, the calculation of $\langle(\boldsymbol{L} \times \boldsymbol{A})_z\rangle$ is straightforward. Integral quantum numbers characterizing the final product are derived from a classical spectrum of values via a 'binning' technique which preserves phase space arguments and has been described in previous works (Lundy *et al* 1994, Lundy and Olson 1995). The scattering angle is defined in terms of the resulting momentum vector of the projectile. In general, 10^4 to 10^5 trials at each impact energy were required for adequate statistical results.

3. Total and differential cross sections for $H^+ + Na(3s, 3p)$

Figure 1 benchmarks CTMC calculations of the total capture cross sections arising from proton interaction with ground-state sodium. The theoretical results reproduce the general trend exhibited by the experimental measurements with the largest window of discrepancy occurring in the region of the maximum cross section, between 2 and 4 keV. Here, the

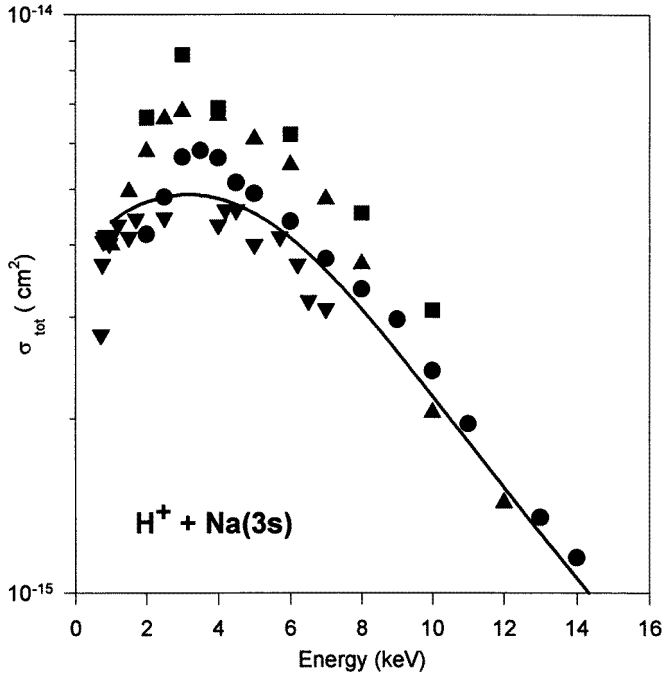

Figure 1. Single-electron capture cross sections for $H^+ + Na(3s)$. CTMC calculations (full curve) are compared to experimental data: circles (Aumayr *et al* 1987), squares (DuBois and Toburen 1985), triangles (Anderson *et al* 1979) and inverted triangles (Nagata 1982).

CTMC curve peaks just below 5×10^{-15} cm^2 in good agreement with the results of Nagata (1982) but 20–30% lower than the measurements of Aumayr *et al* (1987) and Anderson *et al* (1979). From this region of high capture probability to the high-energy limit of this study (15 keV), the predicted cross section drops five-fold.

Examining the n-level product states for collisions with Na(3s) and Na(3p), our theoretical calculations show that at 1 keV only approximately 10% of the captured electrons lie above the first excited energy level; this increases to roughly 50% at 15 keV (figure 2). The available experimental results (Royer *et al* 1988) for state-selective capture are confined to low energies below 3 keV where the classical theory begins to break down due to the strong molecular nature of low-energy collisions. This is more problematic for capture to the lower lying energy states where the electronic energy transition is large and the force acting on the electron by the projectile dominates the interaction. Nevertheless, comparison of the CTMC results for capture from Na(3s) to H($n \geqslant 3$) and from Na(3p) to H($n = 2$) and H($n \geqslant 3$) is to scale with data from Royer *et al*. Moreover, similar investigation of cross-sectional data differential in scattering angle at 2 keV shows good agreement between classical predictions and the measurements of Richter *et al* (1993), figure 3. The nature of these collisions is predominantly long-range soft collisions, whereby the electron is preferentially captured into the $n = 2$ energy level. However, at intermediate energies where stronger coupling between the reaction channels occurs, capture events with higher n-levels increase in probability (figure 2). For the ground-state sodium target, CTMC calculations of the H(2p) populations differential in scattering angle for impact energies 2, 3.5 and 5 keV are displayed in figure 4 along with the experimental results of Roller-Lutz *et al* (1993).

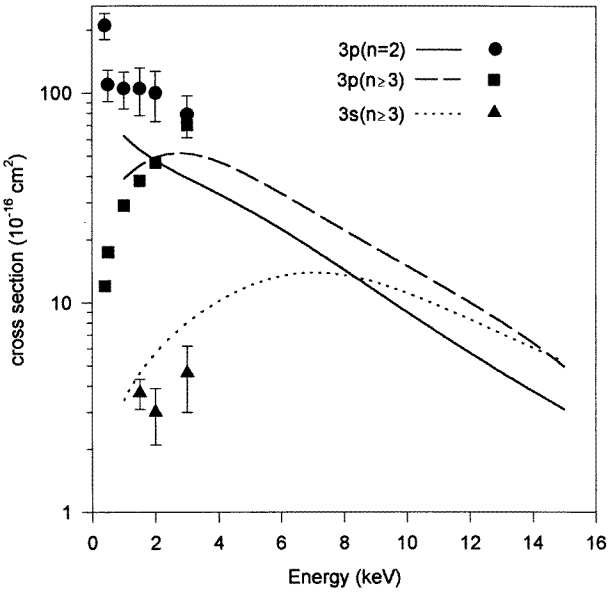

Figure 2. Absolute capture cross sections for H($n \geqslant 3$) production from $H^+ + Na(3s)$ and for H($n = 2$) and H($n \geqslant 3$) generated from $H^+ + Na(3p)$ collisions. $H^+ + Na(3s) \rightarrow H(n \geqslant 3) + Na^+$: CTMC (dotted curve); experiment (triangles). $H^+ + Na(3p)$: H($n = 2$) production, CTMC (full curve); experiment (circles) and H($n \geqslant 3$) production, CTMC (broken curve); experiment (squares). Experimental data from Royer *et al* (1988).

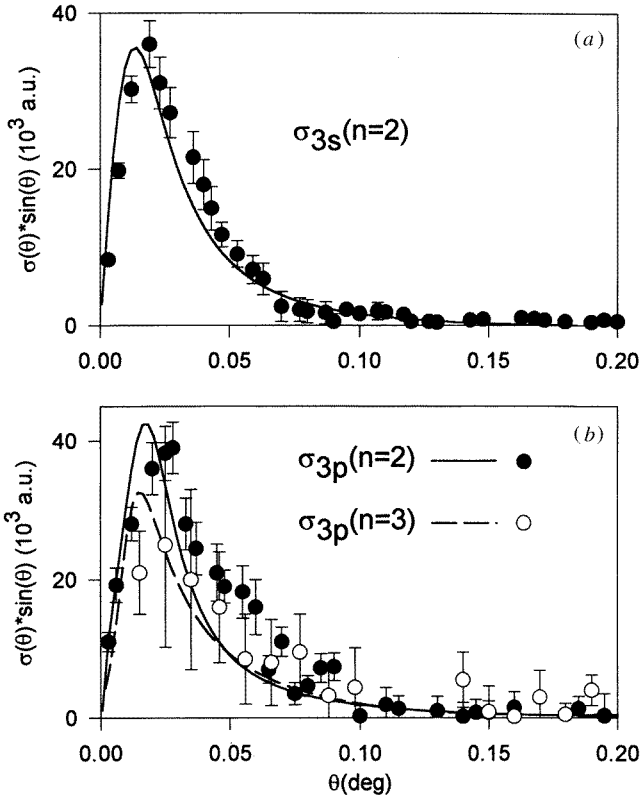

Figure 3. Capture cross sections differential in scattering angle for the reactions $H^+ + Na(3s) \rightarrow H(n = 2) + Na^+$ and $H^+ + Na(3p) \rightarrow H(n = 2, 3)$ at 2 keV. $H^+ + Na(3s) \rightarrow H(n = 2) + Na^+$ (*a*): CTMC (full curve); experiment (full circles). $H^+ + Na(3p)$ (*b*): H($n = 2$) production, CTMC (full curve); experiment (full circles) and H($n = 3$) production, CTMC (broken curve); experiment (open circles). Experimental measurements from Richter *et al* (1993).

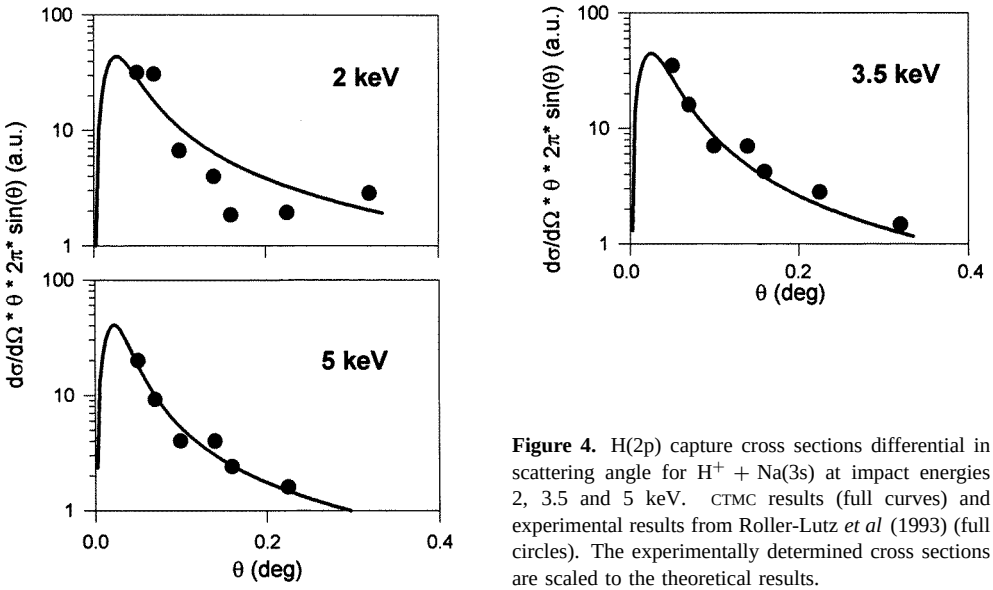

Figure 4. H(2p) capture cross sections differential in scattering angle for $H^+ + Na(3s)$ at impact energies 2, 3.5 and 5 keV. CTMC results (full curves) and experimental results from Roller-Lutz *et al* (1993) (full circles). The experimentally determined cross sections are scaled to the theoretical results.

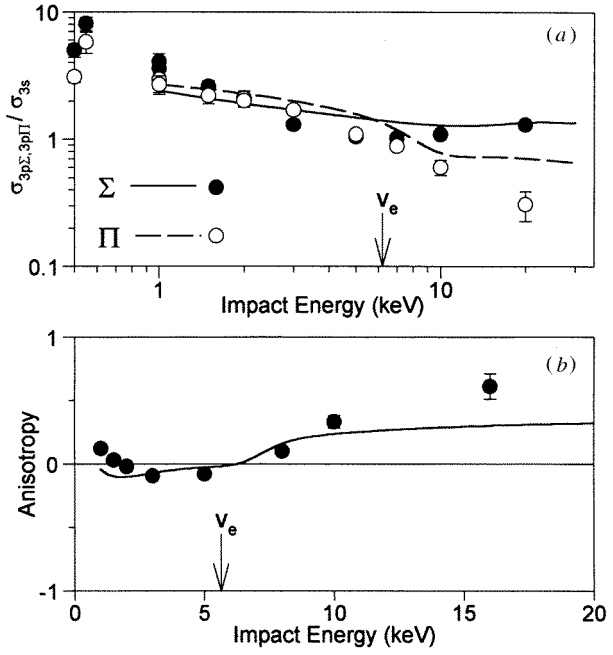

Figure 5. The ratio of total capture cross sections for $H^+ + Na(3p\Sigma, 3p\Pi)$ to the capture cross sections for $H^+ +$ Na(3s) and the anisotropy parameter as a function of impact energy. (*a*) $\sigma_{3p\Sigma}/\sigma_{3s}$, CTMC (full curve); experiment (full circles) and $\sigma_{3p\Pi}/\sigma_{3s}$, CTMC (broken curve); experiment (open circles). (*b*) Anisotropy parameter, CTMC (full curve); experiment (full circles). Experimental results from Müller *et al* (1995). Arrows point to the Na(3p) velocity-matching energy.

4. Anisotropy results for total capture and ionization

The alignment dependence for electron capture to all n-levels is given in figure 5 where cross sections arising from excited, aligned initial states are presented as a ratio to the ground-state results. Experimental observations from Müller *et al* (1995) indicate an increased likelihood of capture from the Na(3pΣ) state below 2 keV and above 6 keV, seen clearly by plotting the energy dependence of the anisotropy parameter (figure 5). According to calculations

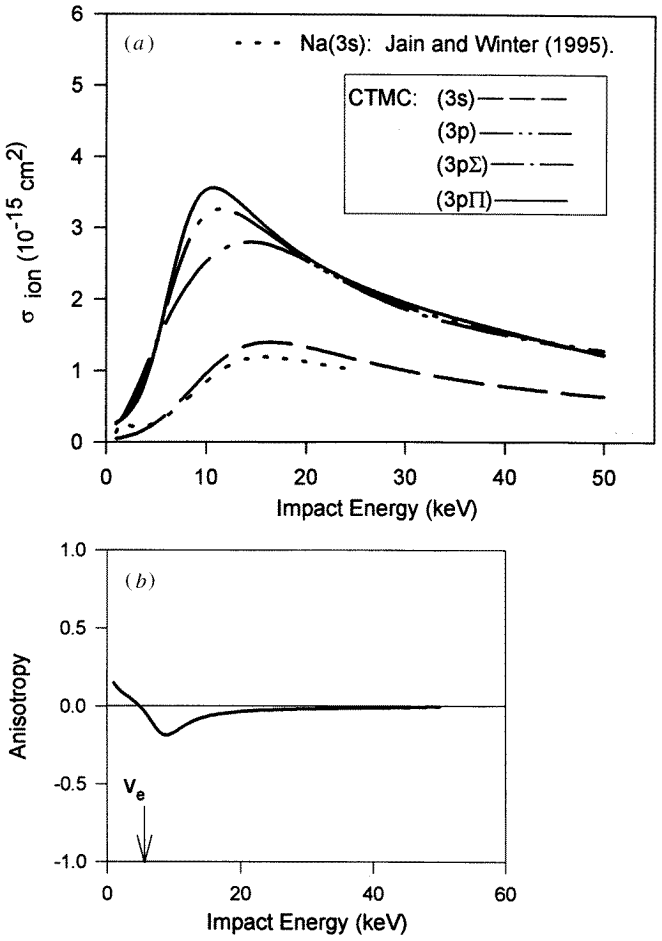

Figure 6. Ionization cross sections and anisotropy parameter. (*a*): CTMC ionization cross sections for H^+ collisions with Na(3s) (– – –), Na(3p) (— ·· —), Na(3pΣ) (— · —), and Na(3pΠ) (——); quantum mechanical calculations (· · · · · ·) from Jain and Winter (1995). (*b*): Anisotropy parameter, CTMC (full curve). Arrow indicates the velocity-matching energy for the Na(3p) electron.

from the CTMC method, an alignment perpendicular (3pΠ) to the incident velocity is slightly favoured for energies below the velocity-matching energy of the Na(3p) electron. At 3 keV the ratio of σ_Π to σ_Σ is roughly 6:5; this becomes 4:7 at 15 keV. Conceptually, this can be viewed in terms of spatial overlap—that is, the large impact-parameter range of low energies increases the probability of electron capture from the (3pΠ) state because of a closer proximity to the impinging projectile. Above 6 keV, collisions occur near the target core where greater spatial overlap exists for the (3pΣ) state. Such reasoning, however, fails to account for the experimental results below 2 keV and does not treat the differing anisotropic behaviour with respect to capture to specific energy levels, but rather an average over those *n*-levels.

Similar anisotropy effects are observed for the ionization channel. In figure 6, classical calculations of ionization cross sections from initial states (3s), (3pΣ) and (3pΠ) show that the maximum probability of ionizing the target electron occurs for the (3pΠ) state near 11 keV. The cross sections corresponding to the parallel alignment $\sigma_{3p\Sigma}$ and the spherically symmetric ground state σ_{3s} peak around 15 keV and are 22% and 61%, respectively, less than the maximum of $\sigma_{3p\Pi}$. The ground-state calculations are in favourable agreement with the quantum mechanical results of Jain and Winter (1995) with a roughly 8% relative difference beyond 15 keV. The anisotropy parameter exhibits a transition near

the velocity-matching energy of 5.7 keV. Below this energy, interaction with the target Na(3pΣ) is more likely to induce ionized electrons; this may be due to some radius-locking effect inherent to the molecular nature of low-energy collisions. Above 5.7 keV, ionization preference is given to the initial Na(3pΠ) state until around 50 keV where the cross sections from the two possible alignments converge. Such energetic collisions occur close to the target core whereby charge-state alignment plays no significant role in the reaction. Instead, it is the binding energy of the target electron which determines the dominance of the ionization channel at these high energies. Such behaviour is illustrated by the plot of anisotropy versus impact energy for ionization of $Na^*(3p)$ (figure 6).

5. State-selective anisotropy results

A probe of energy levels arising from single-electron capture reveals varying anisotropic effects depending upon the n-level (figure 7). For the first excited energy level, CTMC calculations diverge from the low-energy measurements of Dowek *et al* (1990) which have $\sigma_{3p\Sigma}(n = 2)$ dominating over $\sigma_{3p\Pi}(n = 2)$ by a 3:2 ratio. In examining the corresponding scaled cross sections at 1 keV, the theoretical results fall below experimental observations (Richter *et al* 1990) by 55% for $\sigma_{3p\Sigma}$ and 26% for $\sigma_{3p\Pi}$; but this becomes 31% and 2%, respectively, at 2 keV. At 10 keV, CTMC predictions have $\sigma_{3p\Sigma}(n = 2)$ favoured over

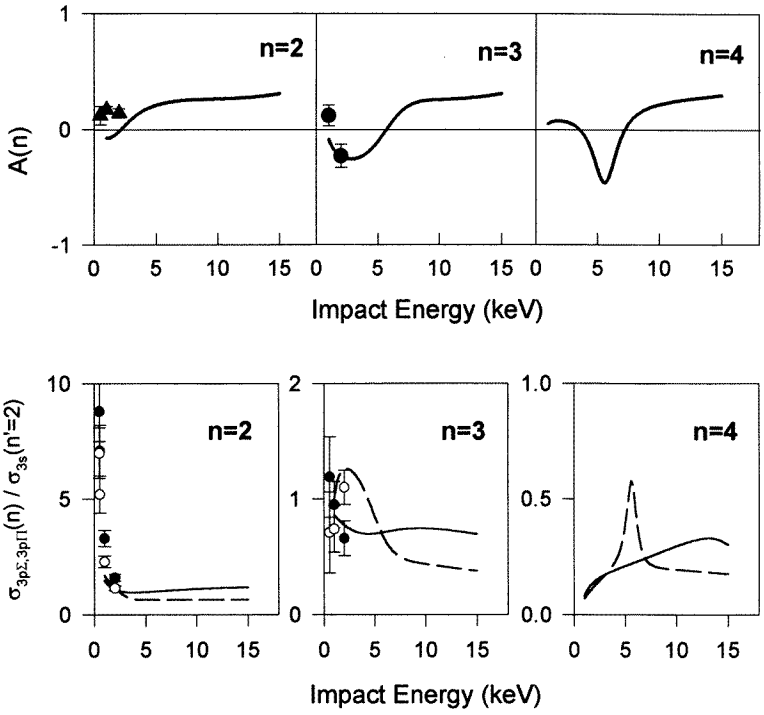

Figure 7. State-selective capture cross sections for $H^+ + Na(3p\Sigma, 3p\Pi)$ scaled to the cross sections for $H^+ + Na(3s) \rightarrow H(n = 2) + Na^+$ and anisotropy parameters. Top graphs: Anisotropy parameters for capture to $n = 2$, 3 and 4, CTMC (full curves); experimental results of Royer *et al* (1988) ($n = 2$: triangles) and ($n = 3$: circles). Bottom graphs: $\sigma_{3p\Sigma}/\sigma_{3s}$, CTMC (full curves); experiment (full circles) and $\sigma_{3p\Pi}/\sigma_{3s}$, CTMC (broken curves); experiment (open circles). Experimental results from Richter *et al* (1990).

Table 1. Theoretical comparison of cross sections (in units of 10^{-16} cm^2) between CTMC and 36-state coupled channel calculations (CCS) (Müller *et al* 1995) for electron transfer into the $n = 2$, 3 and 4 levels and summed over all n-levels (Σ) resulting from proton collisions at energies 2, 5, 10 and 15 keV with Na(3s), Na(3pΣ) and Na(3pΠ) initial states.

Energy (keV)	Final state H(n)	Initial state 3s		3pΣ		3pΠ	
		CTMC	CCS	CTMC	CCS	CTMC	CCS
2	2	41.1	38.9	43.8	73.4	50	45.6
	3	4.34	6.27	32	34.6	65.3	38.2
	4	0.736	3.15	7.5	6.63	5.88	4.22
	(Σ)	47.8	48.4	88.7	114.6	108	88.1
5	2	33	44.4	31.3	37.6	17.1	19.9
	3	8.39	10.6	21.7	17.5	30	28.1
	4	1.43	2.43	5.29	3.81	12	2.78
	(Σ)	45.1	57.9	64.5	59.1	67.9	50.8
10	2	11	13.6	11.8	12.5	5.53	4.05
	3	5.46	6.25	8.04	9.67	3.91	5.33
	4	1.99	1.81	3.3	1.11	2.11	1.84
	(Σ)	22.1	21.9	28.6	24.1	17.6	11.3
15	2	3.73	4.16	4.65	4.22	2.2	1.06
	3	1.9	2.66	3.02	4.13	1.45	1.29
	4	0.928	1.14	1.33	0.865	0.746	0.797
	(Σ)	9.04	8.29	11.8	9.78	6.51	3.18

$\sigma_{3p\Pi}(n = 2)$ by 8:5. Similar relative behaviour is observed for $n = 3$ and $n = 4$ at and above 10 keV with $\sigma_{3p\Sigma}$ dominating. For both $n = 3$ and $n = 4$, a definite minimum is evident in the anisotropy curves. This minimum occurs near 3 keV for $n = 3$ and shifts to 6 keV for $n = 4$. The shift calculated for $n = 3$ agrees with the limited experimental data available. Coupled channel calculations of Müller *et al* (1995) also agree with the CTMC results with respect to the location and depth of the minima in the $n = 3$ and $n = 4$ anisotropy curves. A comparison of the classical and quantum mechanical results is given in table 1.

6. Coherence parameters for the post-collision product

The magnetic sublevel m_ℓ of the captured electrons from an ensemble of trajectories governs the shape of the electronic distribution. Besides the alignment parameter A_{20}, an alternative description of the (2p)-state alignment is the λ parameter which is the ratio of the $m_\ell = 0$ population to the total (2p) population. For collisions involving scattering from Na(3s) targets, the λ parameter, the average of the magnitude of $\boldsymbol{L}_y$, and the alignment angle γ differential in scattering angle are presented in figure 8 along with the experimental measurements of Roller-Lutz *et al* (1993). The primary source of H(2p) comes from long-range collisions generating small scattering angles. Furthermore, these products have a definite preference for population of the $m_\ell = 0$ sublevel—that is, the collision is essentially two-dimensional with the projectile capturing electrons whose orbits are in the plane defined by the impact parameter and velocity vectors. This generates large components of angular momentum perpendicular to the scattering plane. This corresponds to small alignment angles (figure 8). Beyond roughly 0.1°, hard scattering from the nuclear core produces equally populated m_ℓ sublevels.

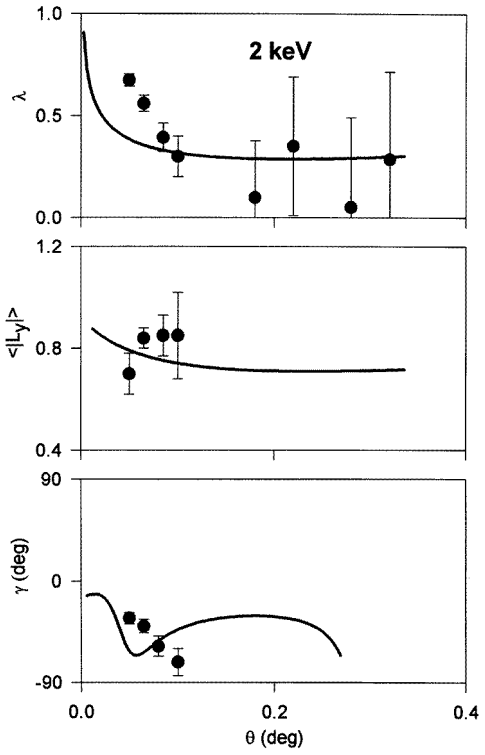

Figure 8. H(2p): λ parameters, $\langle |\boldsymbol{L}_y| \rangle$, and alignment angle γ (deg) differential in scattering angle for $H^+ +$ Na(3s) at impact energies 2 keV. CTMC results (full curves) and experimental results from Roller-Lutz *et al* (1993) (full circles).

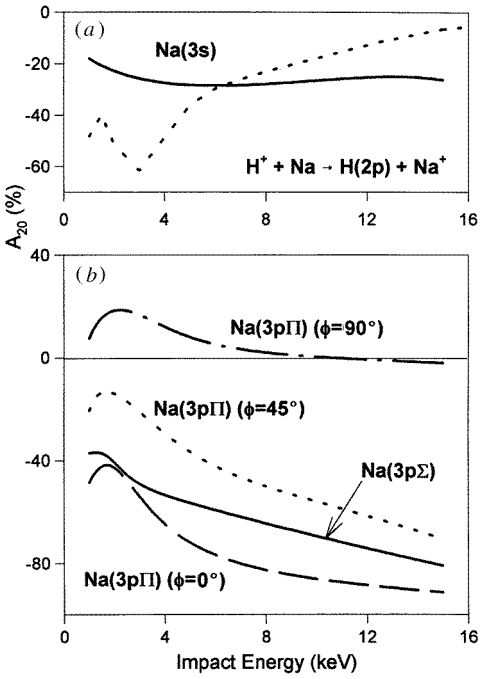

Figure 9. The alignment parameter A_{20} (%) of H(2p) produced from $H^+ +$Na(3s, 3pΣ, 3pΠ) as a function of impact energy. (*a*): Na(3s), CTMC (full curve); quantum mechanical results of Jain and Winter (1995) (dotted curve). (*b*): CTMC results for H(2p) resulting from Na(3pΣ) (full curve), Na(3pΠ) at azimuthal angles $\phi = 0^\circ$ (broken curve), $\phi = 45^\circ$ (dotted curve), and $\phi = 90^\circ$ (chain curve).

In figure 9, CTMC calculations of the A_{20} alignment parameter of H(2p) generated from $H^+ +$ Na(3s, 3pΣ, 3pΠ) collisions exhibit a marked dependence upon the initial target state. When H(2p) is formed from proton interaction with Na(3s), the H(2p) alignment is relatively energy independent. With about -18% to -28% A_{20}, the electronic distribution is favoured along the direction of the collision velocity. The quantum mechanical results of Jain and Winter (1995), however, show a greater energy dependence with the A_{20} parameter essentially going to zero near 15 keV. While quantum mechanics predicts a spherically symmetric charge distribution at 15 keV, the classical description has the electronic cloud elongated parallel to the direction of the collision.

For impact energies greater than 2 keV, classical calculations of A_{20} for H(2p) arising from collisions with excited, aligned Na targets display decreasing values of the alignment parameter. For the Na(3pΣ) initial state, the magnitude of A_{20} more than doubles over the energy range, but A_{20} fails to reach the minimum possible value of -100%. Theoretical calculations of A_{20} for H(2p) arising from Na(3pΠ) with azimuthal angle $\phi = 90^\circ$ show the largest observed value of $+18.7\%$ at 2.3 keV indicating that the axis of the charge cloud is perpendicular to the collision velocity vector. Near 10 keV, the electronic cloud resulting

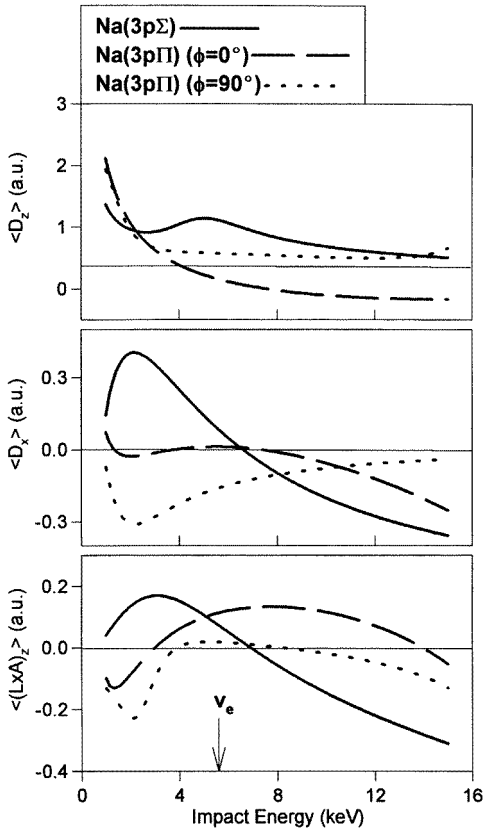

Figure 10. CTMC calculations of coherence parameters $\langle \boldsymbol{D}_x \rangle$, $\langle \boldsymbol{D}_z \rangle$ and $\langle (\boldsymbol{L} \times \boldsymbol{A})_z \rangle$ for H($n = 2$) from $H^+ +$ Na(3pΣ) (full curve) and $H^+ +$ Na(3pΠ) at azimuthal angles $\phi = 0^\circ$ (broken curve) and $\phi = 90^\circ$ (dotted curve). The velocity-matching energy for Na(3p) is indicated by an arrow.

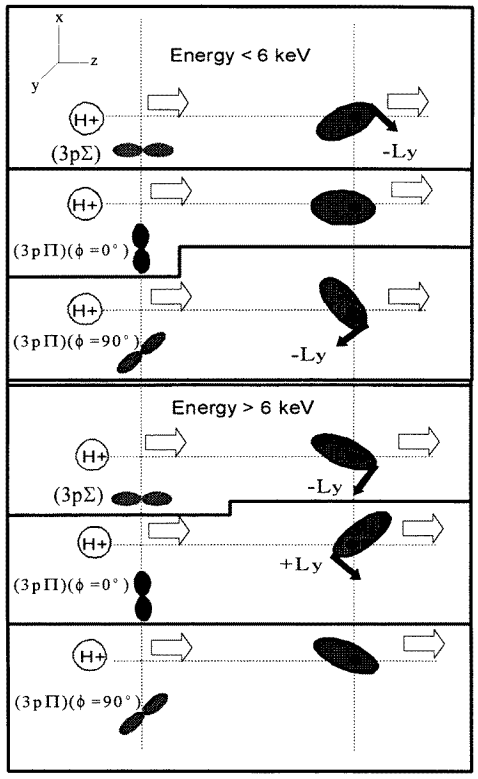

Figure 11. Classical Kepler orbits for H($n = 2$) produced from $H^+ +$ Na(3pΣ), Na(3pΠ) ($\phi = 0^\circ$ and 90°). The direction of collision proceeds along the $+z$-axis. The residual target core is in the lower left-hand corner with respect to the resulting charge cloud. The direction of electronic rotation is indicated by an arrow at the perihelion of the orbit, i.e. the direction of $\langle (\boldsymbol{L} \times \boldsymbol{A}) \rangle$. The top box gives characteristic orbits for impact energies less than 6 keV while the bottom box gives orbits for impact energies greater than 6 keV.

from such an initial distribution becomes spherical. When the charge cloud is rotated towards the x-axis (decreasing ϕ), the alignment of the post-collision product becomes increasingly parallel to the collision direction. With the initial distribution aligned along the x-axis ($\phi = 0^\circ$), the smallest value of $A_{20} = -91.5\%$ results at 15 keV. In this case, H(2p) is almost completely polarized parallel to the impact velocity, even more so than the resulting product from Na(3pΣ). Since (3pΠ) is not a pure state with regard to the magnetic sublevel populations, the alignment of the (2p) state reflects the competition between these sublevels.

The coherence parameters $\langle \boldsymbol{D}_x \rangle$, $\langle \boldsymbol{D}_z \rangle$ and $\langle (\boldsymbol{L} \times \boldsymbol{A})_z \rangle$ for H($n = 2$) are given in figure 10. The sign of $\langle \boldsymbol{D}_x \rangle$ contains information concerning the tilt of the classical orbit in the scattering plane and is with respect to an impinging projectile along the positive x-axis. For the first half of the energy spectrum, $\langle \boldsymbol{D}_x \rangle$ for H($n = 2$) arising from $H^+ +$ Na(3pΣ) is

positive indicating the charge cloud is attracted towards the residual Na^+ target, as shown in figure 11. For $H^+ + Na(3p\Pi)$, $\langle \boldsymbol{D}_x \rangle$ is negative for azimuthal angle $\phi = 90^\circ$ and near zero for $\phi = 0^\circ$. This indicates that the distribution resulting from $Na(3p\Pi)$ ($\phi = 90^\circ$) is tilted away from the Na^+ core while that from $Na(3p\Pi)$ ($\phi = 0^\circ$) has little tilt. $\langle \boldsymbol{D}_z \rangle$ is positive for energies below the velocity-matching energy regardless of the initial alignment of Na(3p); thus, the electronic cloud of $H(n = 2)$ is caught between the two centres. $\langle \boldsymbol{D}_z \rangle$ formed from proton collisions with $Na(3p\Pi)$ ($\phi = 0^\circ$) undergoes a rapid depletion while $\langle \boldsymbol{D}_z \rangle$ corresponding to the initial $Na(3p\Sigma)$ state remains comparatively stable. At energies above the velocity-matching energy, the charge cloud generated from $Na(3p\Pi)$ ($\phi = 0^\circ$) precedes the projectile as if pushed off the target. $\langle (\boldsymbol{L} \times \boldsymbol{A})_z \rangle$ provides information with regard to the orientation of the capture product. The preferred direction of rotation in most cases investigated is such that $\boldsymbol{L}_y$ is negative. One exception to this observation is the counterclockwise rotation for $H(n = 2)$ from $Na(3p\Pi)$ ($\phi = 0^\circ$) at energies above 6 keV. A summary of these results is given by the typical Kepler orbital diagrams in figure 11.

7. Conclusion

We have shown that a classical treatment can be instrumental in analysing the effects of pre-collision alignment of the charge cloud on the post-collision populations as well as on the post-collision alignment and orientation of the capture product. Limitations of the CTMC method may be realized at the low-energy limit of this study where the low projectile charge state and the large impact-parameter range promote a dominating molecular behaviour. Since this method is not restricted by basis set size, examination of high-lying capture levels and high energies where the ionization channel becomes strongly populated is permissible. The results of this study have shown that the initial shape of the electronic distribution plays a significant role in reaction probabilities as well as in the structure of the capture product. The coherence parameters describing the final-state structure provide a rich description of the collision process.

Acknowledgment

This work was supported by a grant from the US Department of Energy, Office of Fusion Energy to the University of Missouri-Rolla.

References

Andersen N, Gallagher J W and Hertel I V 1988 *Phys. Rep.* **165** 1
Andersen N and Hertel I V 1986 *Comments At. Mol. Phys.* **19** 1
Anderson C J, Howald A M and Anderson L W 1979 *Nucl. Instrum. Methods* **165** 583
Aumayr F, Labits G and Winter H 1987 *J. Phys. B: At. Mol. Phys.* **20** 2025
Becker R L and MacKellar A D 1984 *J. Phys. B: At. Mol. Phys.* **17** 3923
Burgdörfer J 1983 *Z. Phys.* A **309** 285
Dowek D, Houver J C, Pommier J, Richter C and Royer T 1990 *Phys. Rev. Lett.* **64** 15
DuBois R D and Toburen L H 1985 *Phys. Rev.* A **31** 3603
Fischer A and Hertel I V 1982 *Z. Phys.* A **304** 103
Garvey R H, Jackman C H and Green A E S 1975 *Phys. Rev.* A **12** 1144
Hertel I V and Stoll W 1978 *Adv. At. Mol. Phys.* **13** 113
Hippler R 1993 *J. Phys. B: At. Mol. Opt. Phys.* **26** 1
Hippler R, Harbich W, Faust M, Lutz H O and Dubé L J 1986 *J. Phys. B: At. Mol. Phys.* **19** 1507
Jain A and Winter T G 1995 *Phys. Rev.* A **51** 2963
Lewartowski E and Courbin C 1992 *J. Phys. B: At. Mol. Opt. Phys.* **25** L63

Lundy C J and Olson R E 1995 *Nucl. Instrum. Methods* B **98** 223
Lundy C J, Olson R E, Schultz D R and Pascale J 1994 *J. Phys. B: At. Mol. Opt. Phys.* **27** 113
Müller U, Meijer H A J, Holme N C R, Kmit M, Lauritsen J H V, Pedersen J O P, Richter C, Thomsen J W, Andersen N and Nielsen S E 1995 *Z. Phys.* D **33** 187
Nagata T 1982 *Mass Spectrosc.* **30** 153
Olson R E and Salop A 1977 *Phys. Rev.* A **33** 3859
Richter C, Andersen N, Brenot J C, Dowek D, Houver J C, Salgado J and Thomsen J W 1993 *J. Phys. B: At. Mol. Opt. Phys.* **26** 723
Richter C, Dowek D, Houver J C and Andersen N 1990 *J. Phys. B: At. Mol. Opt. Phys.* **23** 3925
Roller-Lutz Z, Wang Y, Finck K and Lutz H O 1993 *J. Phys. B: At. Mol. Opt. Phys.* **26** 2697
Royer T, Dowek D, Houver J C, Pommier J and Andersen N 1988 *Z. Phys.* D **10** 45
Schippers S, Boduch P, van Buchem J, Blick F W, Hoekstra R, Morgenstern R and Olson R E 1995 *J. Phys. B: At. Mol. Opt. Phys.* **28** 3271
Schlatmann R, Hoekstra R, Morgenstern R, Olson R E and Pascale J 1993 *Phys. Rev. Lett.* **71** 513
Wang Y, Westphal J, Roller-Lutz Z, Ostrovsky V N and Lutz H O 1994 *Z. Phys.* D **30** 217